JGR Oceans

RESEARCH ARTICLE
10.1029/2021JC017291

Key Points:

- The Chukchi Slope Current is fed by the outflow from Barrow Canyon and a westward jet extending from the southern Beaufort Sea
- The part of the slope current over the upper continental slope continues westward toward the East Siberian Sea
- The slope current overlying deeper isobaths flows northward into the Chukchi Borderland and gets entrained into the Beaufort Gyre

Correspondence to:
H. Leng,
hengling_leng@hotmail.com

Citation:
Leng, H., Spall, M. A., Pickart, R. S., Lin, P., & Bai, X. (2021). Origin and fate of the Chukchi slope current using a numerical model and in-situ data. *Journal of Geophysical Research: Oceans*, *126*, e2021JC017291. https://doi.org/10.1029/2021JC017291

Received 18 FEB 2021
Accepted 26 APR 2021

Origin and Fate of the Chukchi Slope Current Using a Numerical Model and In-Situ Data

Hengling Leng[1,2,3], Michael A. Spall[3], Robert S. Pickart[3], Peigen Lin[3], and Xuezhi Bai[1,2]

[1]Key Laboratory of Marine Hazards Forecasting, Ministry of Natural Resources, Hohai University, Nanjing, China, [2]College of Oceanography, Hohai University, Nanjing, China, [3]Woods Hole Oceanographic Institution, Woods Hole, MA, USA

Abstract A regional coupled sea ice-ocean model and mooring/shipboard measurements are used to investigate the origins, seasonality, and downstream fate of the Chukchi Slope Current (CSC). Three years (2013–2015) of model integration indicates that, in the mean, the model slope current transports ~0.45 Sv of Pacific water northwestward along the Chukchi continental slope. Only 62% of this water emanates from Barrow Canyon, while the rest (38%) is fed by a westward jet extending from the southern Beaufort Sea. The jet merges with the outflow from the canyon, forming the CSC. Due to these two distinct origins, the slope current in the model has a double velocity core at times. This is consistent with the double-core structure of the slope current seen in ship-based observations. Seasonal changes in the volume, heat, and freshwater transports by the slope current appear to be related to the changes in the upstream flows. A tracer diagnostic in the model suggests that the part of the slope current over the upper continental slope continues westward toward the East Siberian Sea, while the portion of the current overlying deeper isobaths flows northward into the Chukchi Borderland, where it ultimately gets entrained into the Beaufort Gyre. Our study provides a detailed and complete picture of the slope current.

Plain Language Summary Water from the Pacific Ocean enters the Arctic domain through the Bering Strait, between the United States and Russia, and subsequently flows northward across the wide and shallow Chukchi Sea. The Pacific-origin water is a critical component of the regional ecosystem and helps set the hydrographic structure of the water column. Previous work suggests that, upon reaching the edge of the Chukchi shelf, much of the water is transported toward the west over the continental slope by the Chukchi Slope Current. However, the precise origin and fate of this current remain uncertain. Using a regional coupled sea ice-ocean model and mooring/shipboard data, we find that the slope current is fed by the outflow from Barrow Canyon in the northeast Chukchi Sea, and also by a westward jet extending from the southern Beaufort Sea. Although some portion of the water advected by the slope current remains on the upper continental slope, as the current overlying deeper isobaths flows northward, part of the water gets entrained into the Beaufort Gyre. These results improve our knowledge of the Pacific water pathways in the Arctic Ocean and would contribute to further understanding of the changing Arctic, such as sea ice loss.

1. Introduction

Pacific water flowing northward through Bering Strait provides a source of heat, freshwater, and nutrients to the Arctic Ocean and plays an important role in the regional hydrographic structure, ecosystem, and climate (Coachman & Barnes, 1961; McLaughlin et al., 1996; Serreze et al., 2006). The freshwater fraction of the Pacific water contributes to the formation of the Arctic halocline, which hinders the heat flux of the Atlantic Water upward to the sea ice base (Aagaard & Carmack 1989; Steele et al. 2004). Over the past decades, the Bering Strait fluxes have shown long-term increases (e.g., Woodgate, 2018; Woodgate et al., 2012). This is suggested to be responsible for recent changes in the western Arctic, including rapid sea-ice retreat (Serreze et al., 2016; Shimada et al., 2006), ocean subsurface warming and freshening (Bourgain & Gascard, 2012; Timmermans et al., 2014), and ocean acidification (Cross et al., 2018; Qi et al., 2017). To achieve a better understanding and prediction of the Arctic changes, better knowledge of the Pacific water pathways is required.

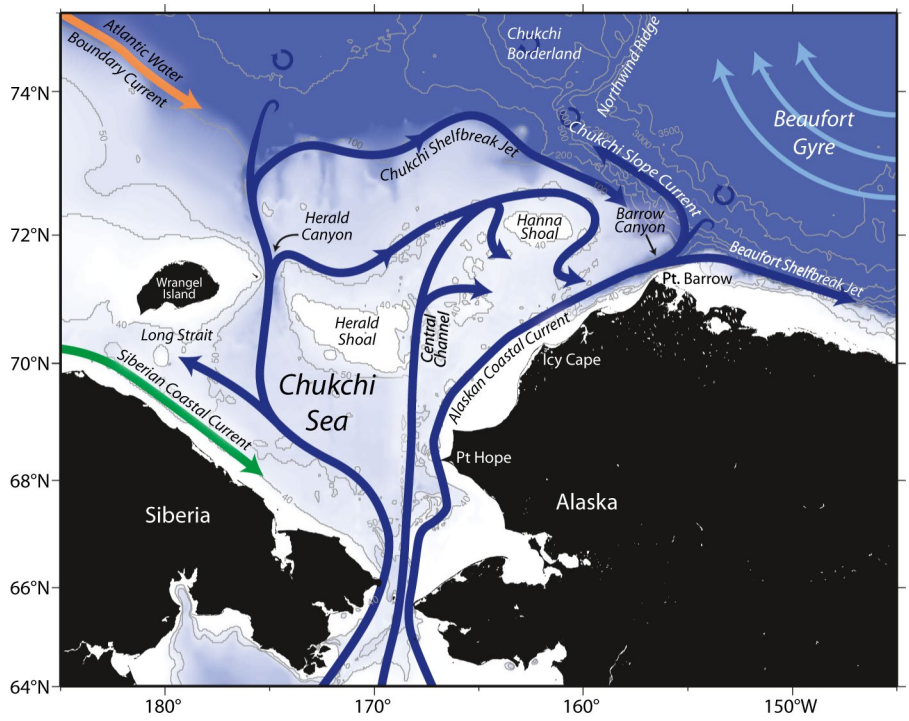

Figure 1. Schematic circulation of the Chukchi and western Beaufort Seas and place names, from Corlett and Pickart (2017). The bathymetry is from ETOPO-2.

In the Chukchi Sea, the Pacific water inflow divides into three main branches (see Figure 1): the western branch into Herald Canyon (Pickart et al., 2010; Woodgate et al., 2005), the Central Channel branch between Herald and Hanna shoals (Weingartner et al., 2005), and the eastern branch along the Alaskan coast (Coachman et al., 1975; Paquette & Bourke, 1974). The presence of these branches is generally supported by numerical models (Panteleev et al., 2010; Spall, 2007; Winsor & Chapman, 2004). Recent observations indicate that part of the western and central branches turns eastward to converge with the eastern branch, which subsequently flows northward through Barrow Canyon (BC) (Fang et al., 2020; Lin et al., 2019; Pickart et al., 2016; Stabeno et al., 2018). Using data from 46 shipboard transects across the Chukchi shelfbreak and slope between 2002 and 2014, Corlett and Pickart (2017) quantified the existence of a westward-flowing current over the continental slope, which transports 0.50 ± 0.07 Sv of Pacific water. This current has been named the Chukchi Slope Current (CSC), and is believed to emanate from the outflow from BC. Further studies based on mooring observations (Li et al., 2019; Stabeno & McCabe, 2020), satellite-tracked drifter/float trajectories (Boury et al., 2020; Stabeno et al., 2018) and numerical models (Spall et al., 2018; Watanabe et al., 2017) support the presence of this current.

The mass budget constructed by Corlett and Pickart (2017) implies that, in the mean, there should be 0.53 ± 0.11 Sv of Pacific water outflowing from BC. This value agrees with the long-term mean result in Itoh et al. (2013) within the error bars, 0.44 ± 0.07 Sv. However, a recent study based on mooring observations concludes that only 0.29 Sv of the Pacific water exiting BC flows westward, providing between ~34% and ~48% of the transport in the slope current (Stabeno & McCabe, 2020). Presently, it is uncertain whether the slope current is fed only by the water from BC or if it has other origins.

The large-scale anticyclonic ocean circulation in the Canada Basin is known as the Beaufort Gyre (BG), and is driven by the anticyclonic wind stress curl associated with the Beaufort High (Proshutinsky et al., 2002). The size and strength of the gyre vary seasonally and interannually in response to changes in the Beaufort High (Proshutinsky et al., 2009, 2002; Regan et al., 2019). Over the period 2003–2014, the gyre expanded northwest toward the Chukchi Borderland with its southern edge residing along the continental slope of the Chukchi and Beaufort Seas (Regan et al., 2019). It has been suggested that the slope current is dynamically related to the BG. In particular, Spall et al. (2018) demonstrated that the slope current can be approximately

regarded as the linear sum of the wind-driven anticyclonic gyre and the outflow from BC. Stabeno and McCabe (2020) argued that the lateral pressure gradient associated with the BG constitutes an effective "wall" along the continental slope to help overcome the restriction of the Coriolis force on the outflow from BC, which results in the westward-flowing slope current. Besides feeding the slope current, a small fraction of the BC outflow turns eastward along the edge of the Beaufort Sea, forming the Beaufort shelfbreak jet (Nikolopoulos et al., 2009; Pickart, 2004).

The model of Watanabe et al. (2017) captured a westward jet (referred to as a "shelfbreak jet") in the winter period extending from the southern Beaufort Sea to the Chukchi slope. Such a westward jet is not found in the two-year mean velocity section from a mooring array deployed across the Alaskan Beaufort shelfbreak and slope (Nikolopoulos et al., 2009). However, during the first year of the array the BG was more extensive than its two-year mean, and a signature of westward flow in the Pacific layer, seaward of the eastward-flowing shelfbreak jet, was evident. The contribution of this westward flow to the CSC has not yet been evaluated.

In addition to the role of the BG in the formation of the CSC, the downstream fate of the current remains unclear. Previous studies based on shipboard transects (Corlett & Pickart, 2017) and drifter trajectories (Stabeno et al., 2018) indicate that the slope current extends as far west as the mouth of Herald Canyon. However, trajectories from a deployment of SOLO floats just west of the canyon revealed a northward pathway of the current after passing the Northwind Ridge (Boury et al., 2020). This suggests that a portion of the Pacific water advected by the slope current can ultimately be entrained into the BG.

In this study, we investigate the origins, seasonality, and downstream fate of the CSC based on a regional coupled sea ice-ocean model and mooring/shipboard observations. The model provides a detailed and complete picture of the slope current and reveals how the Pacific-origin water is transported from the shelves into the interior basin. The model results are supported by the observations. Section 2 gives a description of the model configuration and observational resources. Section 3 evaluates the model results, including the Pacific water fluxes, velocity sections, and hydrographic properties. In Section 4 we describe the relationship between the CSC and upstream flows. In Section 5 the fate of the slope current is discussed. Finally, the main findings of our work are summarized in Section 6.

2. Methods

2.1. Observational Data

We used mooring data collected by the Japan Agency for Marine-Earth Science and Technology (JAMSTEC) to estimate volume, heat (relative to −1.9°C) and freshwater (relative to salinity of 34.8) fluxes through BC. Note that all salinities in the paper are in Practical Salinity Units. The array across the canyon consists of three moorings (BCW, BCC, and BCE), with a spacing of ∼10 km (see locations in Figure 2a). The moorings were configured with conductivity-temperature-depth (CTD) sensors (either Sea-Bird Electronics SBE-16, SBE-37, or SBE-39 recorders), and a combination of acoustic Doppler current profilers (ADCPs) and point current meters for measuring velocity. Details of the data processing are described by Itoh et al. (2013).

The data from a year-long 5-mooring array spanning the shelfbreak and upper-slope of the Chukchi Sea (Figure 2a) were provided by the Bureau of Ocean and Energy Management (BOEM). The spacing between each mooring is ∼11 km. The moorings were equipped with coastal moored profilers (CMPs), MicroCATs, CTDs, and ADCPs providing hydrographic (vertical resolution of 1–2 m) and velocity (vertical resolution of 5–10 m) data from October 2013 to September 2014. A detailed description of the data and processing is given by Li et al. (2019).

Monthly mean values of Bering Strait properties including volume, heat and freshwater fluxes for the period from January 2013 to December 2015 are employed for the model validation. All of the fluxes are calculated from the data of mooring A3 (see the location in Figure 2b) just north of the Bering Strait (Woodgate, 2018; Woodgate et al., 2015).

In addition, the shipboard CTD and ADCP data from 46 sections occupied across the Chukchi shelfbreak and slope, and the resultant absolute geostrophic velocity, employed by Corlett and Pickart (2017), are used to compare to the model results (e.g., the double-core structure of the CSC). The collection of sections

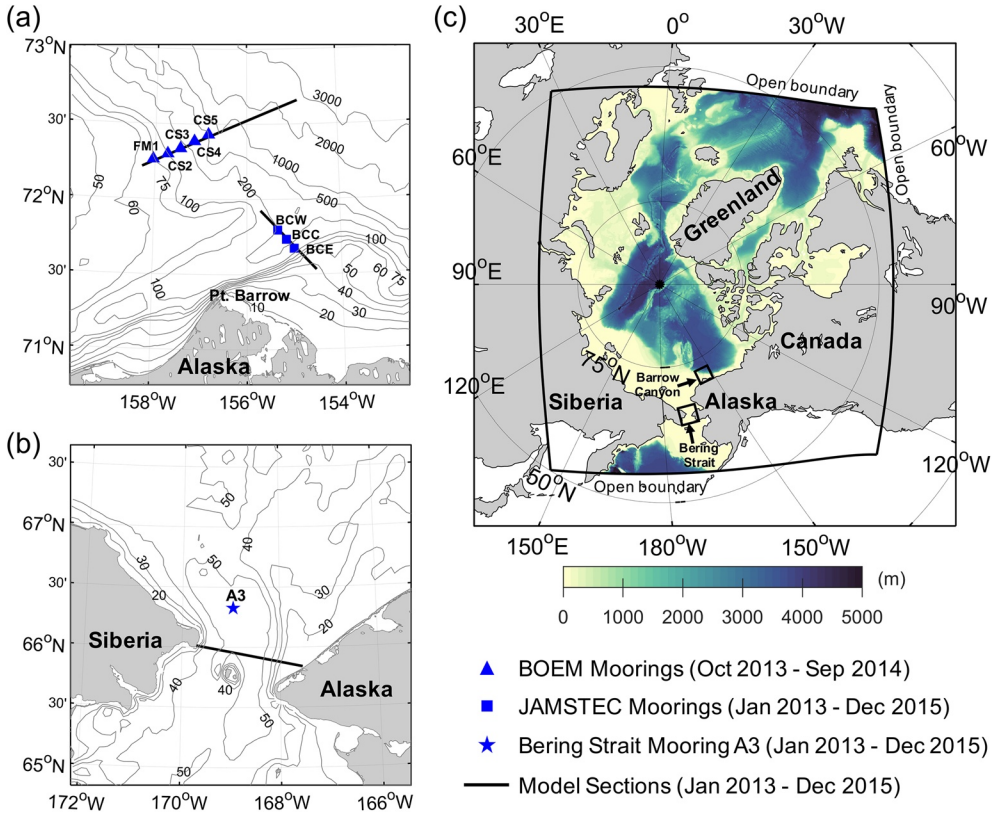

Figure 2. Locations of (a) the BOEM Chukchi shelfbreak and slope moorings and JAMSTEC Barrow Canyon moorings, and (b) Bering Strait mooring A3. BOEM = Bureau of Ocean Energy and Management; JAMSTEC = Japan Agency for Marine-Earth Science and Technology. Black lines in (a and b) indicate model sections. (c) Model domain with three open boundaries and bottom topography. The two black boxes outline the domains in (a and b). The legend shows the time periods of the measurements and model sections.

spanned the time period 2002–2014, during the months of May to October. The data have high spatial resolution (typical station spacing of ~10 km). For details regarding the ship-based data and the calculation of the absolute geostrophic velocities, see Corlett and Pickart (2017).

2.2. Model Description

The model used in this study is a regional coupled sea ice-ocean model based on the Massachusetts Institute of Technology general circulation model (MITgcm) (Marshall et al., 1997). We followed the Arctic configuration given by Nguyen et al. (2012) and modified the vertical levels for a more detailed simulation of the upper ocean. The modified configuration has 71 levels in the vertical, including 40 levels over the upper 300 m. The layer thickness gradually increases from 2 m at the top level to ~450 m at the bottom level (the depth of the bottom layer is ~5,900 m). The model domain covering the Arctic Ocean (Figure 2c) comprises 1,680 by 1,536 cubed-sphere grid cells with a mean horizontal grid spacing of ~4.5 km. Applications of the rescaled vertical coordinate "z*" (Adcroft & Campin, 2004; Campin et al., 2008) and the partial cell formulation of Adcroft et al. (1997) allow for an accurate representation of the bathymetry. The bathymetry is constructed by Nguyen et al. (2012) merging the blend S2004 (Marks & Smith, 2006) with the International Bathymetric Chart of the Arctic Ocean (IBCAO; Jakobsson et al., 2008). The ice model is based on a variant of the viscous-plastic dynamic-thermodynamic sea ice model (Zhang & Hibler, 1997) as described in Losch et al. (2010).

The ocean model utilizes the nonlinear equation of state of Jackett and McDougall (1995). Vertical mixing is parameterized by the nonlocal K-Profile Parameterization (KPP) scheme of Large et al. (1994). Horizontal viscosity of Leith (1996) is modified by Fox-Kemper and Menemenlis (2008) to sense the divergent flow.

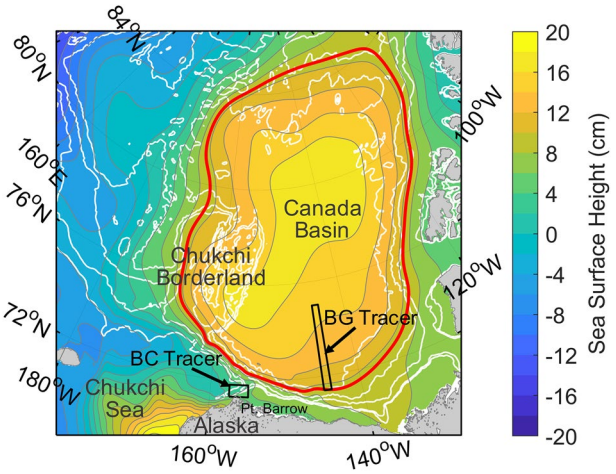

Figure 3. Simulated annual mean sea surface height (cm) in the western Arctic. The red contour indicates the mean edge of Beaufort Gyre, which is defined by the lowest closed contour of the sea surface height, in line with Regan et al. (2019). The two regions of tracer release are indicated by the black boxes. White contours are the 100, 200, 1,000, 2,000, and 3,000 m isobaths.

The nondimensional Leith biharmonic viscosity factor is 1.5 for both the vorticity part and the divergence part. No explicit horizontal diffusivity is required as a seventh-order monotonicity-preserving advection scheme (Daru & Tenaud, 2004) is used. The background vertical diffusivity is intentionally small ($5.44 \times 10^{-7} m^2\ s^{-1}$) in order to accommodate the salt plume parameterization (Nguyen et al., 2009). There is also a quadratic bottom drag with coefficient 2.1×10^{-3}. No surface temperature or salinity restoring is used.

The simulation covers six years from January 2010 to December 2015. Only the output of the last three years was used for analysis. The model is initialized with ocean fields from the Polar Science Center Hydrographic Climatology (PHC) 3.0 (winter fields) (Steele et al., 2001) and sea ice fields from the Polar Science Center Global Sea Ice (GIOMAS) Data Sets (Zhang & Rothrock, 2003). Lateral boundary conditions are monthly means of potential temperature, salinity, and horizonal velocity at three open boundaries (see locations of the boundaries in Figure 2c) extracted from the partially constrained Estimating the Circulation and Climate of the Ocean, Phase II (ECCO2) solution (Menemenlis et al., 2008). Atmospheric forcing components including sea surface wind speed, pressure, temperature, humidity, downward short- and long-wave radiation, and precipitation are derived from the Japanese 55-year Reanalysis (JRA-55; Kobayashi et al., 2015) 6-hourly data set. As the largest contributor of freshwater to the Arctic, river runoff is important in maintaining the stratification and is likely to influence the formation and melt of sea ice (e.g., Bareiss et al., 1999; Nummelin et al., 2015). The monthly mean river runoff used in the model is from the Regional, Electronic, Hydrographic Data Network for the Arctic Region (R-ArcticNET) (Lammers et al., 2001; Shiklomanov et al., 2006).

Two passive tracers were released starting on the 1st of January 2013 to track the pathways of the outflowing water from Barrow Canyon (BC tracer) and the water of the Beaufort Gyre (BG tracer). The BC and BG tracers are continuously set to unity through the entire water column in the canyon and in a narrow band across the Beaufort Sea, respectively, and advected and diffused with no external forcing elsewhere (see Figure 3). The narrow band extends from the mean southern edge of the gyre offshore to the basin interior. The gyre edge is defined by the lowest closed contour of the sea surface height, consistent with Regan et al. (2019).

3. Model Validation

3.1. Fluxes Through Bering Strait and Barrow Canyon

We estimated the annual (2013–2015) mean fluxes and standard deviations through Bering Strait by averaging the monthly mean values from the Bering Strait mooring A3 (Woodgate, 2018; Woodgate et al., 2015). We computed the BC fluxes based on the time series from the JAMSTEC array (Itoh et al., 2013). The fluxes through Bering Strait and BC were also calculated using three-day average model output (the model sections are shown in Figures 2a and 2b) and compared to the observations. Annual mean results are summarized in Table 1 and monthly mean time series are shown in Figure 4.

The annual mean volume transport through Bering Strait is estimated to be 0.99 ± 0.03 Sv (the uncertainty is the standard error) in the model, which agrees well with the observational value (1.11 ± 0.27 Sv). For the same period, the simulated annual mean transport through BC is 0.34 ± 0.03 Sv, in line with the observational result (0.31 ± 0.07 Sv). The model has reasonable heat (11.4 ± 0.7 TW) and freshwater (69 ± 2 mSv) fluxes through Bering Strait compared to the observations (10.6 ± 2.1 TW, 76 ± 19 mSv). However, note that the data from mooring A3 do not capture the Alaskan Coastal Current (ACC) and hence underestimate the heat and freshwater fluxes through the strait (Woodgate, 2018; Woodgate et al., 2015).

The model accurately reproduced seasonal cycles in the volume, heat and freshwater fluxes through Bering Strait and BC (Figure 4). The fluxes through Bering Strait reach their maxima (~1.5 Sv, ~30 TW, and

Table 1
Annual Mean Volume, Heat and Freshwater Fluxes Through Bering Strait and Barrow Canyon for the Period 2013–2015

	Bering Strait (observation)	Bering Strait (model)	Barrow Canyon (observation)	Barrow Canyon (model)
Volume flux (Sv)	1.11±0.27	0.99±0.03	0.31±0.07	0.34±0.03
Heat flux (TW)	10.6±2.1	11.4±0.7	1.5±0.3	1.8±0.2
Freshwater flux (mSv)	76±19	69±2	19±4	23±2

Note: The simulated mean fluxes were calculated from three-day average model output. The observational mean fluxes through Bering strait were estimated by averaging the monthly values from the Bering Strait mooring A3. The observational mean fluxes through Barrow Canyon were calculated using the data from the JAMSTEC array. The reference temperature for the heat flux is −1.9°C and the reference salinity for the freshwater flux is 34.8.

~100 mSv) in summer and minima (~0.7 Sv, ~0 TW, and ~50 mSv) in winter. Due to the presence of the ACC, the fluxes through BC are stronger from July to September, while sometimes they show peaks in other months (e.g., November 2013), which is probably associated with synoptic local wind events (see Itoh

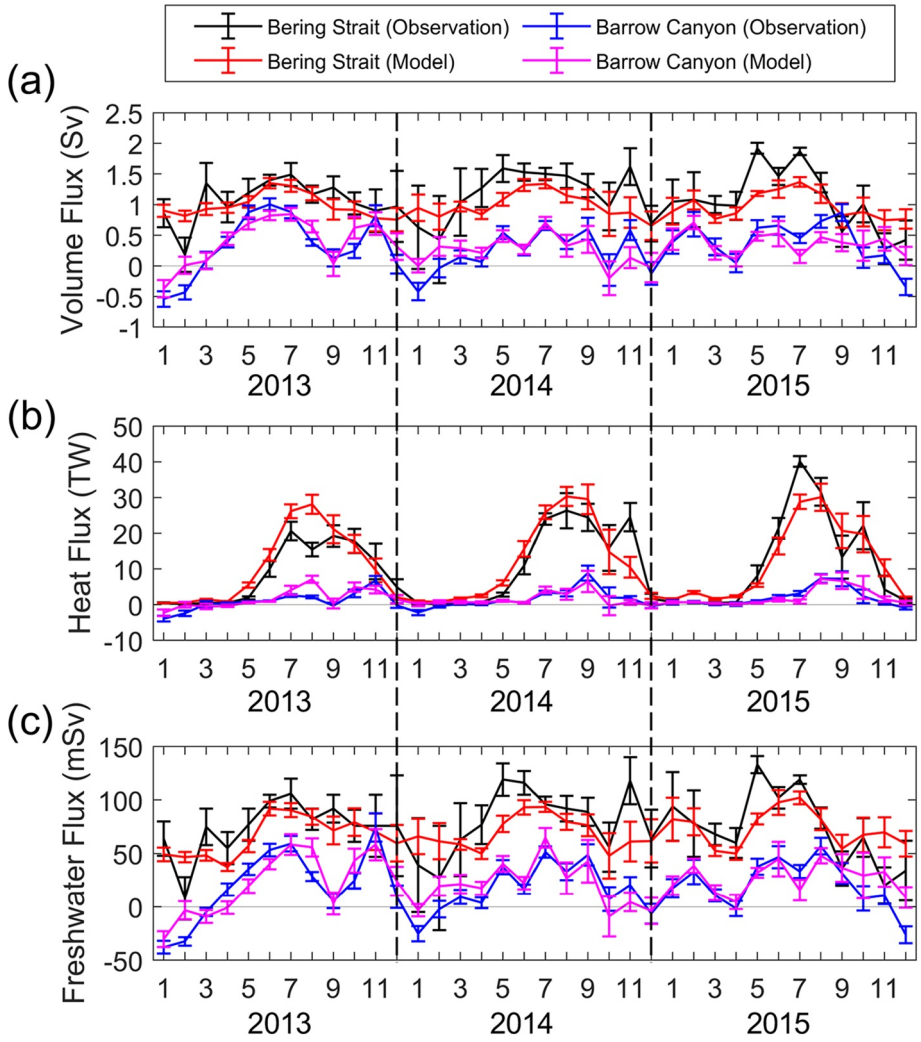

Figure 4. Monthly mean time series of (a) volume, (b) heat and (c) freshwater fluxes through Bering Strait and Barrow Canyon calculated from the mooring observations and model output, respectively. The negative volume flux through Barrow Canyon means a reversed flow (southwestward). The reference temperature for calculating the heat flux is −1.9°C and the reference salinity for the freshwater flux is 34.8.

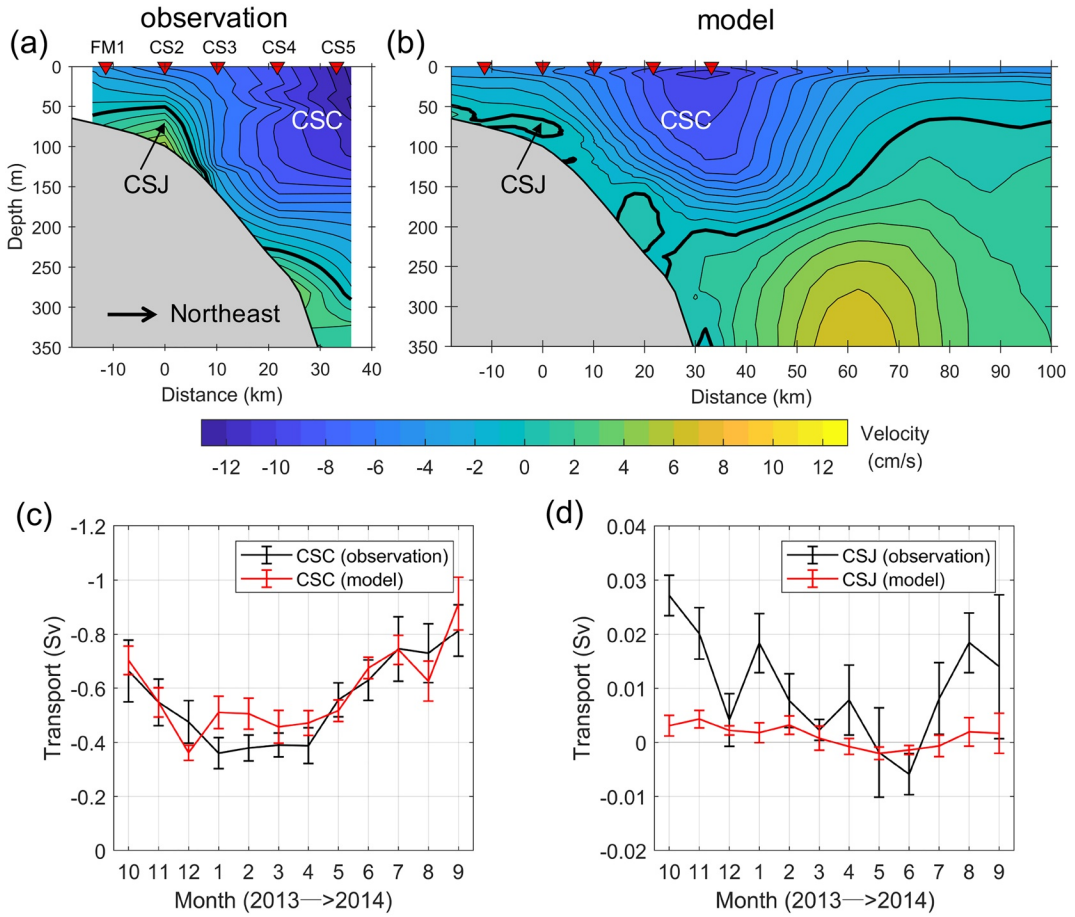

Figure 5. (a) Year-long (10/2013–9/2014) mean alongstream velocity section (positive flow is southeastward) constructed from the Chukchi shelfbreak and slope mooring data. (b) Simulated year-long mean alongstream velocity section for the same period. The offshore distance is relative to the 100 m isobath. Bold black line in (a) and (b) marks the zero-velocity contour. Locations of the mooring sites are indicated above the sections. (c) Monthly mean time series of the volume transport of the Chukchi Slope Current (CSC). (d) Monthly mean time series of the volume transport of the Chukchi shelfbreak jet (CSJ, eastward-flowing portion). Black and red lines in (c and d) indicate the observational and simulated results, respectively.

et al., 2013). In the winter months the BC throughflow is reduced (or even reversed, e.g., January 2013 and January 2014), resulting in the weakest down-canyon (northeastward) fluxes.

3.2. The Chukchi Slope Current

The CSC advects a combination of Pacific water, Atlantic water, and melt water (the melt water in the paper includes runoff, precipitation, and ice melt contributions). The transport component of each water mass can be estimated according to the definitions of the regional water masses in Nikolopoulos et al. (2009) and Corlett and Pickart (2017). Typically, the interface between the Pacific water layer and the Atlantic water layer lies at a salinity (S) of 33.64 and potential temperature (T) of −1.26°C, which corresponds to the depth of maximum Ertel potential vorticity (Nikolopoulos et al., 2009). Note that the hydrographic sensors equipped in the BOEM moorings only measured data below ~50 m; therefore, it is difficult to distinguish the component of melt water from the others using those mooring data. The transports presented below include the contributions due to Pacific water and melt water but exclude the Atlantic water ($S > 33.64$ and $T > -1.26$°C).

Figure 5a shows the year-long (October 2013–September 2014) mean alongstream velocity section constructed from the Chukchi mooring data as in Li et al. (2019). The dominant signal in Figure 5a (from

moorings FM1 to CS5) is the CSC, which flows northwestward and is surface-intensified. The measured year-long mean transport of the slope current between FM1 and CS5 is 0.45 ± 0.03 Sv. This value is an underestimate because the mooring array did not bracket the slope current. For nearly half of the daily sections, the velocity core of the slope current was close to or beyond the edge of the array. To estimate the missing transport in these cases, Li et al. (2019) invoked a "mirroring" technique (taking the offshore part of the current as the mirror image of the inshore part). The resultant "whole" transport of the slope current is 0.57 ± 0.04 Sv, which agrees well with the independent estimate of Corlett and Pickart (2017) in which the current was fully bracketed. The mean section of Figure 5a also reveals two southeastward flows: one is the bottom-intensified Chukchi shelfbreak jet centered near CS2 (distance between −20 and 10 km) and the other is the inshore portion of the Atlantic water boundary current system (distance between 20 and 40 km, deeper than 200 m).

The simulated year-long (October 2013–September 2014) mean velocity section is shown in Figure 5b, which extends offshore to a distance of 100 km (relative to the 100 m isobath). The slope current in the model has similar features as in the observations, such as the velocity structure (compare Figures 5a and 5b) and volume transport (Figure 5c). The current is enhanced in summer/fall and becomes weaker during winter/spring. The measured transport of the slope current varies between 0.3 and 0.9 Sv, reaching a peak in September. The year-long mean simulated slope current transport is 0.59 ± 0.02 Sv, consistent with the observational estimate (0.57 ± 0.04 Sv). However, the transport of the slope current between FM1 and CS5 in the model is only 0.34 ± 0.02 Sv, lower than the measured value between these two moorings (0.45 ± 0.03 Sv). This is due to the model current being wider than in the mooring observations. The simulated transport of melt water in the slope current is 0.08 Sv; excluding that from the total transport yields the contribution from Pacific water, which is 0.51 Sv. This value is nearly identical to the estimate of 0.50 ± 0.07 Sv by Corlett and Pickart (2017) using the collection of shipboard transects during the summer months (July–October).

The Chukchi shelfbreak jet is not well resolved in the model, probably due to the limit of the resolution. It may also be weak because the model has too much transport across the shelf into the interior (this is discussed below in Section 6). The simulated year-long mean transport of the shelfbreak jet is only 0.001 Sv, much smaller than the observational value (0.009 ± 0.003 Sv). Figure 5d indicates that the simulated shelfbreak jet is weak in all months.

The model reproduced a similar seasonal cycle in the velocity structure of the slope current compared to the observations (Figure 6). The current is surface-intensified in summer/fall, and becomes middepth-intensified in spring. However, the model does not capture the subsurface velocity maximum in winter (compare Figure 6h with Figure 6g).

A detailed description of the seasonality of water masses in the slope current was given in Li et al. (2019). They found a continued presence of the newly ventilated Winter Water (NVWW, $S > 31.5$ and $T < -1.6$°C) from early April to late-July, in the depth range 50–170 m (Figure 7a). The model also captured the NVWW during the same period, although most of it appeared at depths shallower than 50 m (Figure 7b). The Pacific summer waters, including Bering Summer Water (BSW, $30 < S < 33.6$ and $0 < T < 3$°C) and ACW ($30 < S < 32$ and $T > 3$°C) were barely detected in the shipboard sections in July and August but became significant in September (Corlett & Pickart, 2017), which is also seen in Figure 7b. The top floats of the Chukchi shelfbreak and slope moorings were situated at 50 m, therefore the mooring data do not extend to the depth range of ACC, and thus there is no ACW in Figure 7a. Only a small portion of BSW was present deeper than 50 m depth.

4. Relationship Between the Chukchi Slope Current and Upstream Flows

4.1. Origins of the Chukchi Slope Current

Note that there is significant interannual variability in the BC throughflow (see Figure 9 in Itoh et al., 2013). In some years (e.g., 2002, 2003, and 2006), the mean transport through the canyon was larger than 0.50 Sv; however, in 2001 and 2007 the values were only 0.24 and 0.35 Sv, respectively. As noted above in Section 3.1, the BC throughflow was generally smaller during the period 2013–2015, which suggests that there was not enough transport during this time period to account for the full CSC. Accordingly, this implies there should

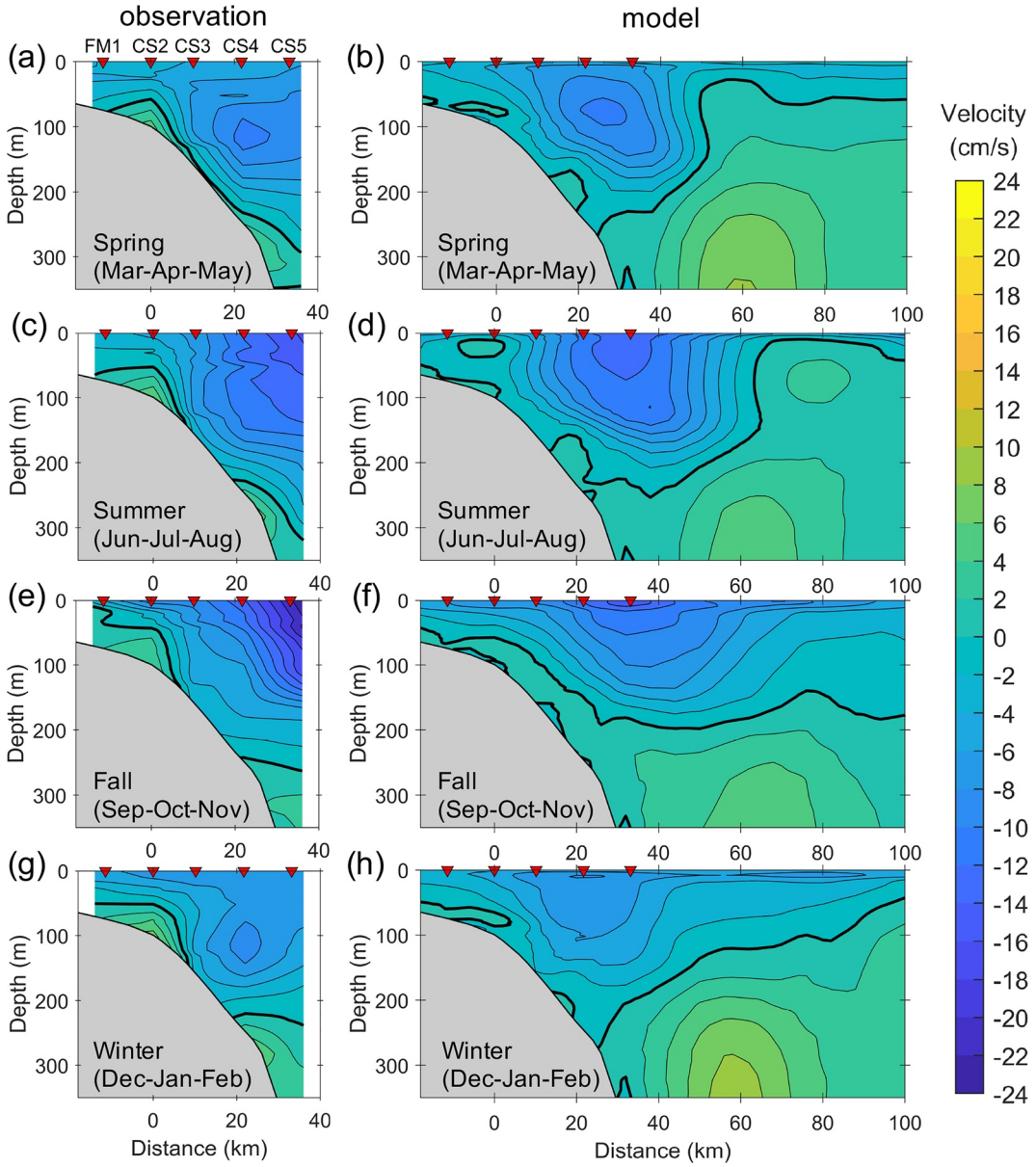

Figure 6. Vertical sections of the seasonally averaged alongstream velocity: (left) constructed from the Chukchi shelfbreak and slope mooring data and (right) from the model. The presentation is the same as in Figures 5a and 5b.

be another source of water to the slope current, in the density range of Pacific water, supplementing the outflow from BC. This is the case in the model.

As seen in Figure 8, a westward jet extends from the Beaufort slope (between ~1,000 and 3,000 m isobaths) to the Chukchi slope (contrary to the eastward-flowing Beaufort shelfbreak jet shown in Figure 1). This merges with the outflow from the canyon to form the CSC. This westward jet on the Beaufort slope is quite similar to the simulated jet in Watanabe et al. (2017), although their simulations focused on the winter period when the BC throughflow was reduced or even reversed (see their Figure 10). In that case the slope current (referred to as a "shelfbreak jet" in Watanabe et al., 2017) was mainly fed by the water from the east. Based on our three years of model output, this feature is present year-round and is evident in the annual mean velocity fields (Figure 8).

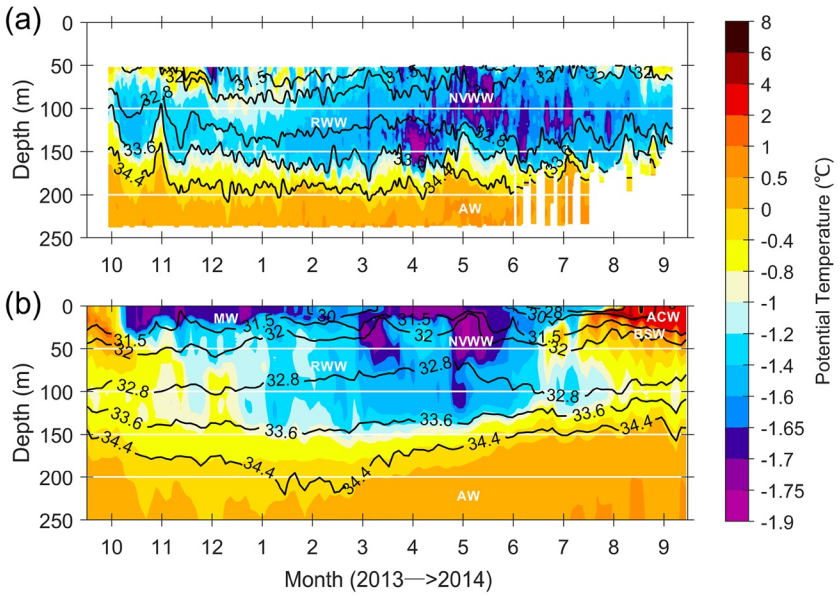

Figure 7. Depth-time plot of potential temperature (color) overlain by salinity contours at mooring CS4 (see Figure 5a): (a) from the mooring data using a 3-day low-pass filter, and (b) from three-day average model output. The white contours mark 50 m depth increments for ease of comparison. Major water masses are labeled: MW = Melt Water; ACW = Alaskan Coastal Water; BSW = Bering Summer Water; RWW = Remnant Winter Water; NVWW = newly-ventilated Winter Water; AW = Atlantic Water.

In the southern Beaufort Sea, the main part of the westward jet resides offshore of the 1,000 m isobath (Figure 8). Onshore of this is the eastward-flowing Beaufort shelfbreak jet (between ~50 and 100 m isobaths). A mooring array deployed across the Beaufort shelfbreak and slope from August 2002 to September 2004 showed that the Beaufort shelfbreak jet is trapped to the shelfbreak near 100 m depth with a width of 10–15 km (Nikolopoulos et al., 2009). The array extended offshore to the 1,400 m isobath. While the two-year mean flow was directed eastward across the full array, throughout most of the first year there was westward flow seaward of the 250 m isobath. The BG expanded farther south that year than in the second year, which likely explains why the mooring array measured this westward flow. Presumably the flow continued to the Chukchi continental slope, consistent with Figure 8.

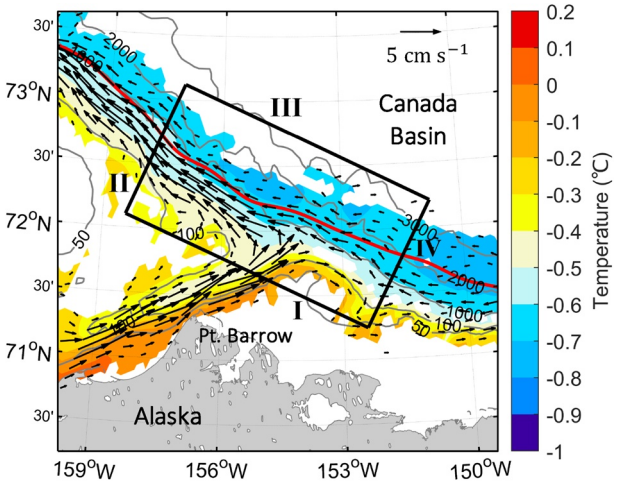

Figure 8. Annual mean temperature (color) and horizontal velocity (vectors) faster than 0.5 $\mathrm{cm\,s^{-1}}$ averaged over the salinity range $30 < S < 33.6$. The red line indicates the mean edge of the Beaufort Gyre (see Figure 3 for the entire contour). Four sections (I, II, III, and IV) form a box for calculating the volume, heat, and freshwater budgets of the Pacific water.

Further evidence for the view that the slope current has two distinct origins is that a double-core structure is sometimes seen in the model velocity sections (see the cases in Figures 9a and 9b). Such a double-core structure was also present in the observational summer mean section in Corlett and Pickart (2017) (Figure 9c) and in the simulated winter section in Watanabe et al. (2017). Using the same shipboard data as in Corlett and Pickart (2017), we calculate the transport of Pacific water in the inner core to be 0.29 Sv, constituting 58% of the total Pacific water transport (0.50 Sv) in the slope current. The remaining fraction (0.21 Sv) is in the outer core, which accounts for 42%.

4.2. Volume, Heat, and Freshwater Budgets

To quantify the contributions of the two distinct origins of the slope current, we calculated the volume, heat, and freshwater budgets in a box centered at the mouth of BC using the three years of model output (Figure 8). The box is comprised of four vertical sections, extending from sea surface down to a depth of 350 m. Melt water and Atlantic water were

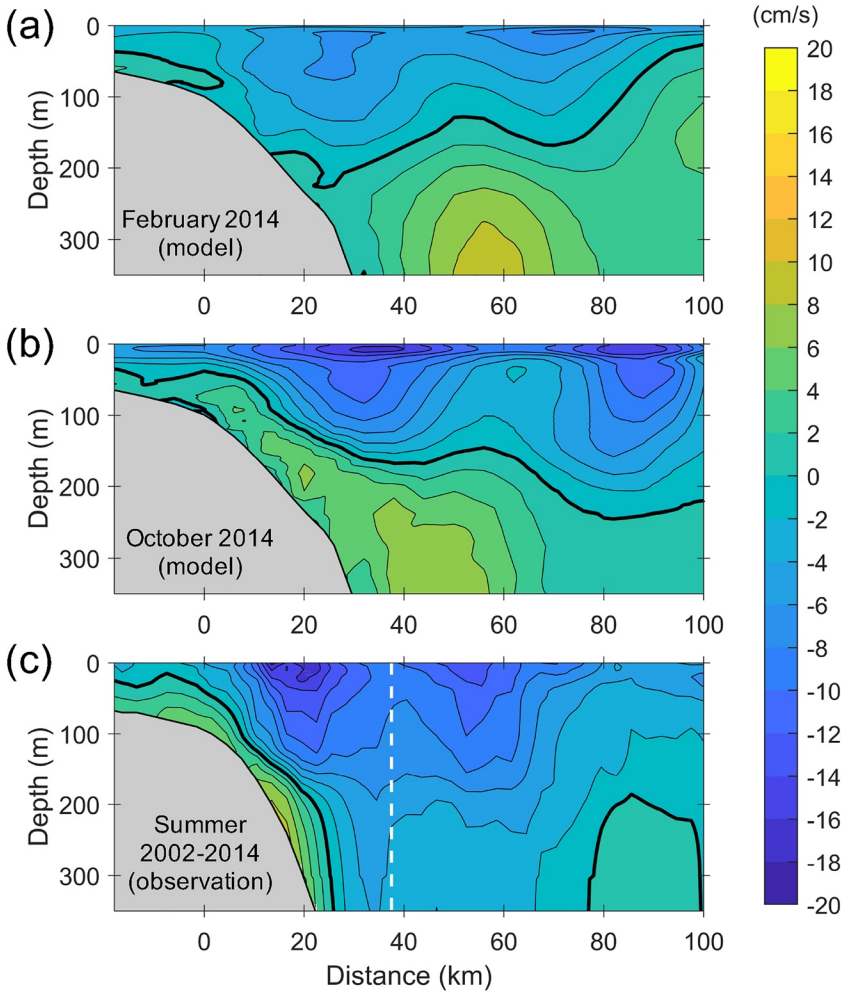

Figure 9. (a and b) Two cases of the Chukchi Slope Current velocity section with a double-core structure from the model. The location of the section is shown in Figure 2a (black line along the BOEM mooring array). (c) Summertime mean velocity section of the Chukchi Slope Current, from Corlett and Pickart (2017), showing the double-core structure. The white dashed line shows the division for calculating the transport in each core.

excluded in the calculations so as to focus on the advection of Pacific-origin water. Vertical exchange between the Pacific water layer and Atlantic water layer was not considered.

In the mean, the export in the slope current (Section II) is estimated to be 0.45 Sv (Figure 10a), which is equal to the sum of the inputs through Section I (0.32 Sv) and Section IV (0.13 Sv). Approximately 0.28 Sv (not shown) of the Pacific water exiting BC turns west to feed the slope current, while 0.04 Sv flows eastward along the edge of the Beaufort Sea and crosses Section IV. Accordingly, the transport in the westward jet is 0.17 Sv (0.13 Sv + 0.04 Sv). With these values, we deduce that the BC outflow provides ~62% (0.28/0.45) of the Pacific water transport in the slope current, and the westward jet from the Beaufort slope contributes 38% (0.17/0.45). These proportions correspond well to those of the two cores in the summertime mean section from Corlett and Pickart (2017) (as given in Section 4.1). As such, the double-core structure of the slope current can be attributed to the two distinct origins.

Figure 10b shows that the heat flux through the canyon (1.8 TW) is three times that from the east (0.6 TW). Most of the heat is exported to the west by the slope current (1.9 TW), while the rest is lost through sea surface (0.4 TW, equivalent to 15 $\mathrm{W\,m^{-2}}$) for melting ice or exchange with the atmosphere. The BC outflow carries 22 mSv of freshwater into the box contributing to about two-thirds of the freshwater export in the slope current, twice that from the east (11 mSv) (Figure 10c). The export to the basin interior through Section III

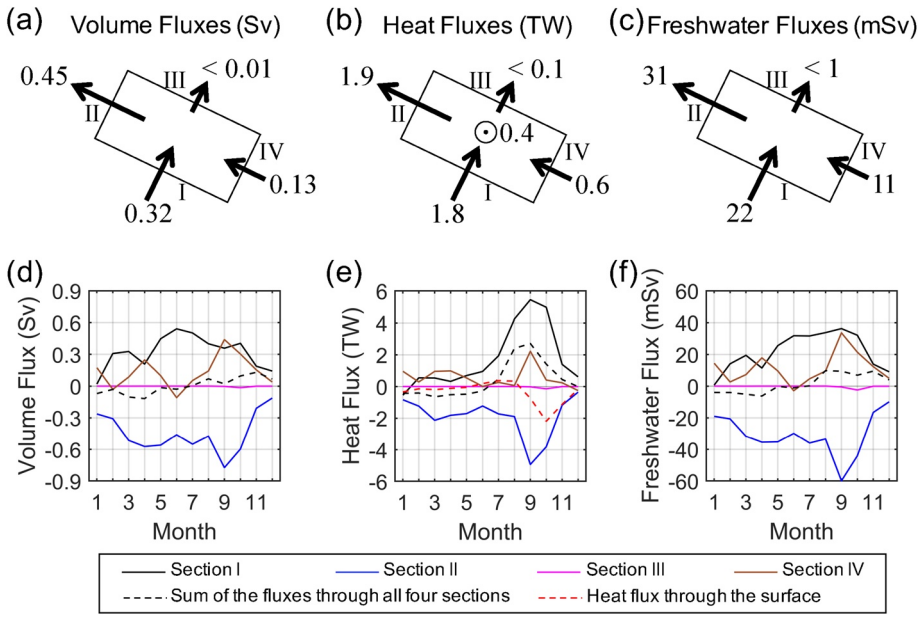

Figure 10. (a–c) Annual mean (black arrows) and (d–f) monthly mean time series of volume, heat, and freshwater fluxes through the four sections shown in Figure 8. Positive (negative) values indicate fluxes into (out of) the box. All of the fluxes exclude the contributions due to melt water and Atlantic water. The heat flux through the surface is considered in (b) (circle dot-symbol) and (e) (red dashed line).

is smaller than 1 mSv. Note that the lateral fluxes through the four sections (with consideration of heat flux through surface) are approximately conserved, indicating that vertical exchange between the Pacific and Atlantic water layers is relatively small.

The outflow from BC (Section I) (Figure 10d, black solid line) exhibits a larger seasonal cycle than the export in the CSC (Section II) (Figure 10d, blue solid line). This is because of the contribution from the westward jet (Section IV) (Figure 10d, brown solid line), which shows two peaks during the year (spring and fall). Due to the joint contribution of the BC outflow and the westward jet, the export in the slope current reaches a peak in September, three months later than the peak transport in the canyon. A similar delay in the peak transport of the slope current versus the BC outflow was previously discussed by Spall et al. (2018) based on a high-resolution regional model. Note, however, that their model does not show the westward jet. Rather, they argued that the delay in the peak transport of the slope current versus the BC outflow is due to the partitioning of the BC outflow between the westward slope current and eastward Beaufort shelfbreak jet, due to the seasonal change in stratification.

Seasonal changes in the freshwater fluxes (Figure 10f) are dictated by the volume flux (Figure 10d) except for Section I. Although the volume flux through the canyon starts to decline after the peak in June, the freshwater flux remains large until late fall due to the presence of ACC (note that the contribution of melt water has been excluded in the calculations). It is known that the surface-intensified ACC is present during summer and fall, which transports warm and fresh ACW through BC (Itoh et al., 2013). In response to the large heat/freshwater flux through BC, the heat/freshwater transport by the slope current shows a pronounced peak in September (Figures 10e and 10f, blue solid lines). We also found a net heat input to the box through lateral advection from July to December, which was then lost through the surface for melting ice or exchange with the atmosphere. The peak heat loss from the surface (Figure 10e, red dashed line) lags the peak in the lateral heat input (Figure 10e, black dashed line) by one month.

4.3. Seasonal Change of the Velocity Structure

Based on the year-long mooring array, Li et al. (2019) documented that the slope current changes seasonally from being surface-intensified in summer/fall (Figures 6c and 6e) to middepth-intensified in winter/spring

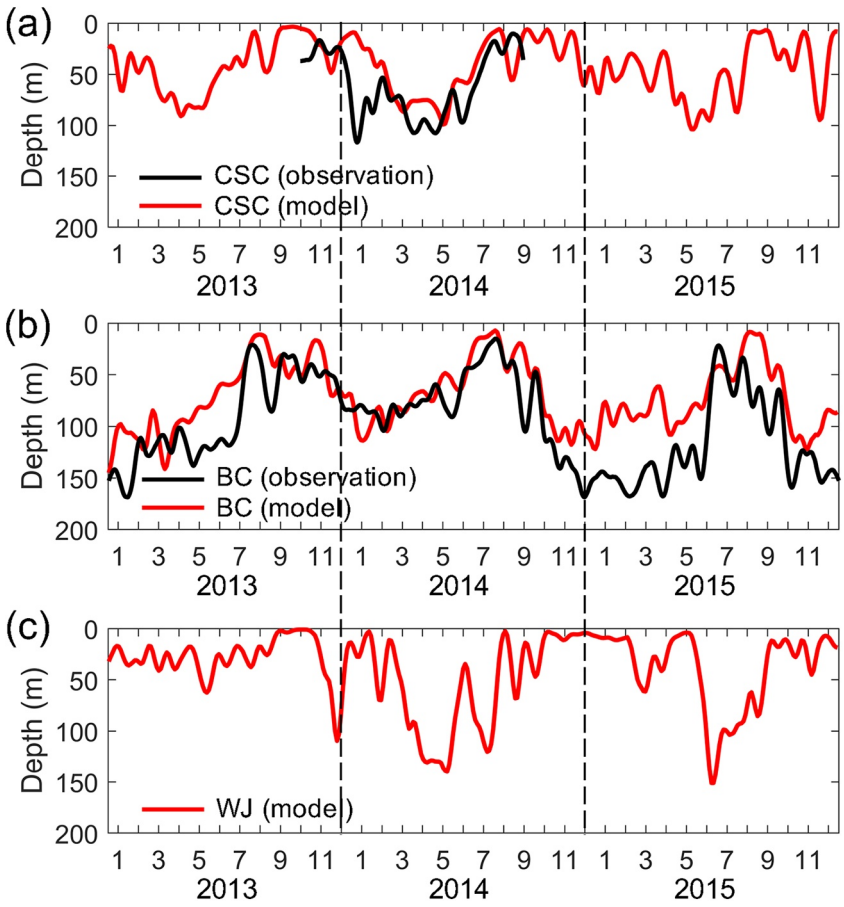

Figure 11. Thirty-day smoothed time series of the depth of the velocity maximum in (a) the Chukchi Slope Current (CSC), (b) the outflow from Barrow Canyon (BC), and (c) the westward jet (WJ, through Section IV in Figure 8). Bold black lines in (a and b) are from the mooring observations. Bold red line in each panel is the model result.

(Figures 6a and 6g). To document the seasonal change of the slope current structure, we present time series of the depth of the maximum velocity (Figures 11a). The model reproduced a similar seasonal cycle in the slope current compared to the mooring observations from October 2013 to September 2014, although it did not capture the subsurface core in the 2013/14 winter. A comparable seasonal cycle was reproduced in all three model years.

The vertical shift of the velocity maximum is more significant in the outflow from BC (Figure 11b). The flow has a subsurface core for most of the year (from November to June) and becomes surface-intensified in late summer and early fall. The core varies between 0–180 m depth. This is in line with the mooring observations between October 2006 and September 2007 (Itoh et al., 2013). The surface-intensified flow in summer/fall through BC is due to the presence of the ACC. In the cold months the ACC disappears, and the flow in the canyon has a middepth maximum.

Given the similarity between Figures 11a and 11b in the changing depths of the velocity core, one might think that the changing structure of the slope current is being dictated by the flow through BC. We note, however, that the other origin of the slope current, the westward jet on the Beaufort slope, shifts vertically as well (Figure 11c). Based on numerical results, Watanabe et al. (2017) argued that the structure of the westward jet is associated with the local isopycnal fronts trapped by the steep seafloor topography. They suggested that the depression of upper isohalines on the shelf side due to shelf water intrusion should be responsible for the subsurface core in the westward jet (via geostrophic set up). However, the model of Spall et al. (2018) shows no evidence of cross-shelf transport broadly distributed along the Chukchi shelfbreak. These two contrasting numerical results raise the question of whether and how the shelf water can cross

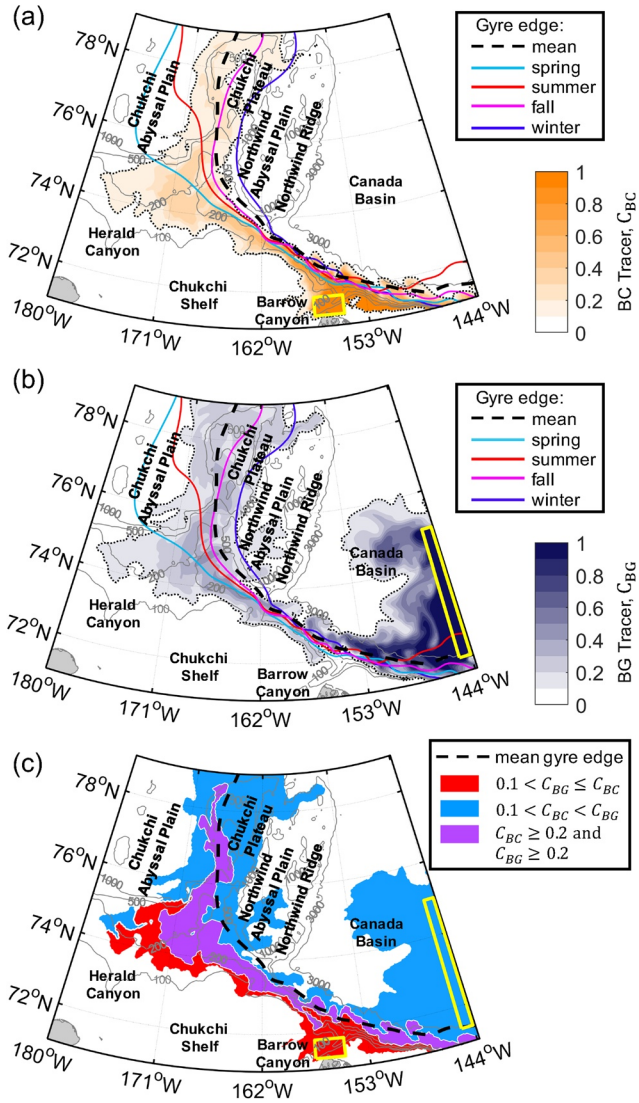

Figure 12. Snapshots of (a) Barrow Canyon outflow water tracer (BC tracer, C_{BC}) and (b) Beaufort Gyre water tracer (BG tracer, C_{BG}) at 50 m depth at the end of 2013. The dotted contours in (a and b) show the edges of BC and BG tracers defined by the concentration of 0.1. The bold dashed contour indicates the annual mean edge of the Beaufort Gyre. Solid colored contours indicate the gyre edges for the four seasons. (c) Three regions with different tracer characteristics: $0.1 < C_{BG} \leq C_{BC}$ (red), $0.1 < C_{BC} < C_{BG}$ (blue), and $C_{BC} \geq 0.2$ and $C_{BG} \geq 0.2$ (purple). The yellow boxes indicate the regions of tracer release.

the Chukchi shelfbreak to help set the subsurface core in the slope current. Although our model produces more cross-shelf transport than in the model of Spall et al. (2018), there is no evidence that the depression of upper isohalines on the shelf side is related to the intrusion of shelf water. Further work is needed to determine whether the seasonal change of the slope current structure is dominated by the upstream flows or local forcing.

5. Fate of the Slope Current

The fate of the CSC and its relationship to the BG are diagnosed by considering two passive tracers: the BC tracer released in Barrow Canyon and the BG tracer released in the gyre (see the description in Section 2.2). Figures 12a and 12b shows snapshots of the two passive tracers at the depth of 50 m at the end of 2013. The distribution of the BC tracer reveals two main pathways of the Pacific-origin water after exiting Barrow Canyon. The eastward branch is the Beaufort shelfbreak jet and the westward one is the CSC. The BC tracer in the slope current follows bathymetry toward the Chukchi Borderland, then much of it proceeds northwest onto the Chukchi Plateau after passing the Northwind Ridge. This is consistent with the trajectories of SOLO floats (drogue depth 80–100 m) presented in Boury et al. (2020) which proceeded northward along the eastern edge of the plateau. However, the shipboard sections analyzed by Corlett and Pickart (2017) and near-surface (25–30 m) drifter trajectories presented by Stabeno et al. (2018) indicate that the slope current resides on the upper continental slope and continues westward toward the East Siberian Sea. These results suggest two different fates of the slope current.

Boury et al. (2020) noted that the deeper isobaths of the Chukchi slope west of Northwind Ridge veer more northward than the shallower ones. They argued that if the slope current is located over relatively shallow depths it would continue westward, while in the cases when it is in deeper water it would be more apt to flow northward. Our tracer results support this view. As seen in Figure 12a, part of the BC tracer remains on the upper continental slope in the vicinity of the 200 m isobath, progressing westward to the mouth of Herald Canyon.

The fate of the BC tracer is also dependent on the water depth at which it resides. At a depth of 30 m much of the tracer spreads to the west (Figure 13a), while at 80 m most of it flows northward onto the Chukchi Plateau (Figure 13b). The BC tracer entering the Chukchi Plateau spread further widely around the Chukchi Borderland at the ends of 2014 and 2015 (Figures 13c and 13d). This indicates that at least part of the water in the slope current ultimately gets entrained into the BG, as hypothesized by Boury et al. (2020). On the other hand, a considerable part of the BC tracer remains on the upper continental slope, verifying the presence of the westward branch of the slope current after passing the Northwind Ridge (Corlett & Pickart, 2017; Stabeno et al., 2018).

The BG tracer is advected to the west by the gyre and much of it crosses the mean edge of the gyre into the Beaufort/Chukchi slope region (Figure 12b). We defined three regions based on the tracer distributions (Figure 12c). The narrow region in red is dominated by the BC tracer ($0.1 < C_{BG} \leq C_{BC}$), which extends from the Beaufort shelfbreak westward to the mouth of Herald Canyon. The region in blue is dominated by the BG tracer ($0.1 < C_{BC} < C_{BG}$) with its main portion located within the southern edge of the gyre. In between the two is the transition region (in purple), where both the BC and BG tracers are larger than 0.2.

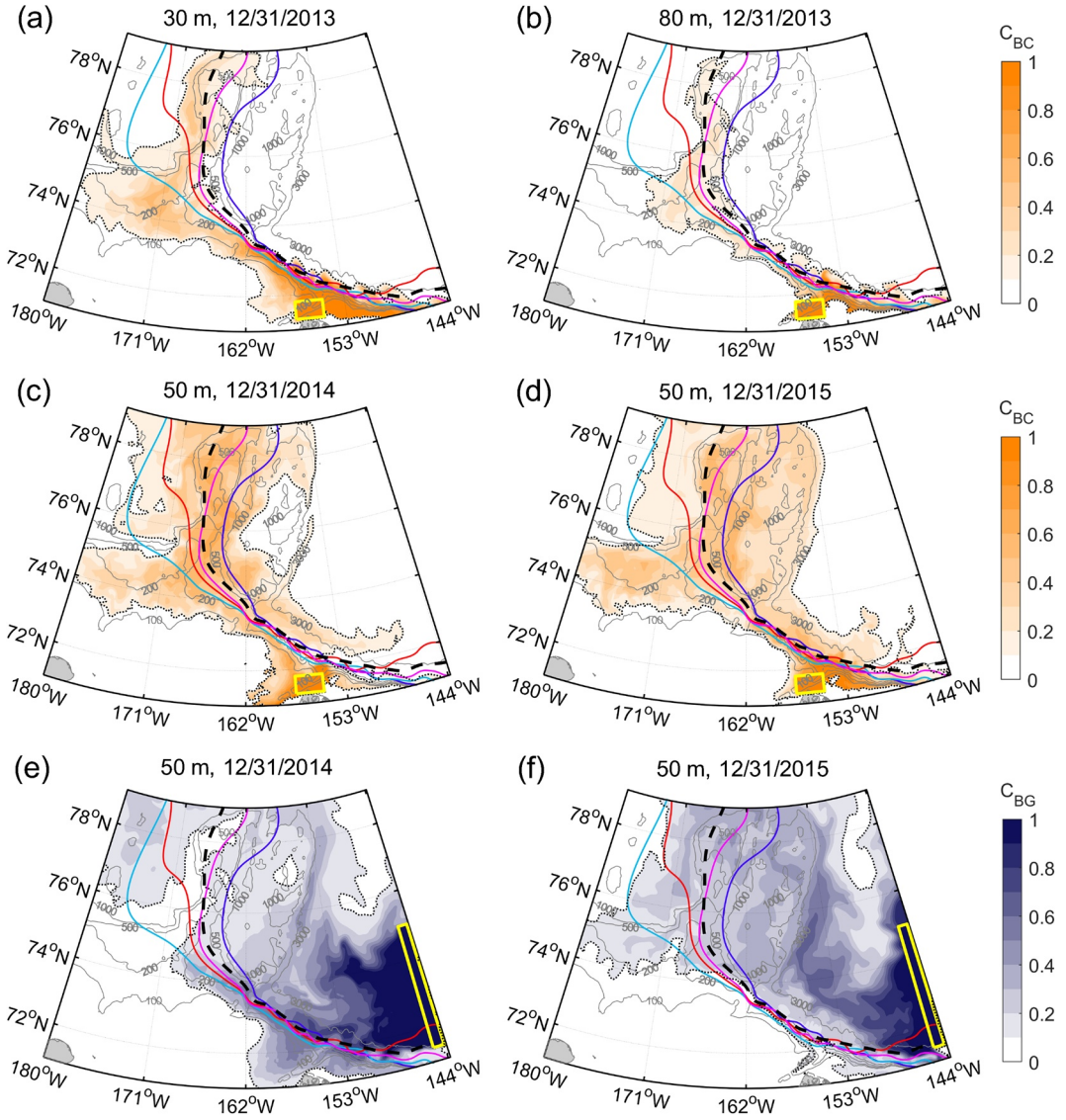

Figure 13. (a and b) Same as Figure 12a but at 30 and 80 m depths. (c and d) Same as Figure 12a but at the ends of 2014 and 2015. (e and f) Same as Figure 12b but at the ends of 2014 and 2015.

Notably, the purple transition region extends all the way along the gyre edge until north of Chukchi Plateau. This indicates that the slope current contains waters from both Barrow Canyon and the southern Beaufort Sea (offshore of the Beaufort shelfbreak). As mentioned above in Section 4, the westward jet extending from the Beaufort slope merges the outflow from Barrow Canyon to form the CSC, such that the transition region on the Chukchi slope is more or less controlled by these two upstream flows. Since the two upstream flows have different seasonal variations in transporting the Pacific water (see Figure 10d), their relative influence on the transition region should be time-dependent.

The pathways of the slope current west of the Northwind Ridge are far from Barrow Canyon, and thus are more likely to be controlled by the topography and the BG. As seen in Figure 12c, there is an onshore expansion of the transition area southwest of the Northwind Abyssal Plain, where the lateral shift of the gyre edge is significant. In winter the western edge of the gyre was located nearby the Chukchi Plateau, while in spring it shifted westward to the Chukchi Abyssal Plain. Note that the seasonal variability of the BG in the model is somewhat different from the satellite observations (2003–2014) presented in Regan et al. (2019). For example, the observational western edge of the gyre was nearby the Chukchi Plateau in summer and

shifted to the Chukchi Abyssal Plain in fall (see their Figure 3). This might be due to the different time periods. The southern edge of the gyre shifts onshore/offshore as well, although it is constrained by the bathymetry. Furthermore, meanders and mesoscale eddies are common in the slope region (Corlett & Pickart, 2017; Zhao et al., 2014), which is conducive to the exchange between the gyre and the slope current.

6. Summary and Discussion

In this study, we have investigated the origins, seasonality, and downstream fate of the CSC using a regional coupled sea ice-ocean model and mooring/shipboard observations. The model showed the year-round presence of the westward-flowing slope current, consistent with the observations. The simulated transport, velocity structure, and water mass properties in the slope current also agree qualitatively with the observational results.

Our simulations indicate that the slope current has two distinct origins. One is the outflow from Barrow Canyon, known to be driven by the Bering Strait inflow, providing ~60% of the Pacific water transport in the slope current. The other is a westward jet extending from the southern Beaufort Sea (seaward of the eastward-flowing Beaufort shelfbreak jet), which contributes 40% of the slope current transport. This westward jet is evident at times in mooring data from the Beaufort slope (Nikolopoulos et al., 2009) and is also present in the simulated winter section of Watanabe et al. (2017). Our results also explain the double-core structure of the slope current in the mean shipboard section from Corlett and Pickart (2017), in that the proportions of the inner and outer cores correspond well to those of the Barrow Canyon outflow and the westward jet. The volume, heat, and freshwater transports of the slope current vary seasonally and reach their peaks in September, which is related to the seasonal changes in the upstream flows. In addition, the seasonally varying depth of the velocity core of the slope current appears to be primarily dictated by what is flowing through Barrow Canyon, although it is also likely to be affected by local forcing as argued by Watanabe et al. (2017).

The simulated westward jet on the Beaufort slope can be regarded as a part of the BG, considering that the main portion of the jet stems from the gyre farther to the east (not shown), that is, it is supplied by the gyre. On the other hand, part of the westward jet resides outside the gyre edge (Figure 8) and is likely to be fed by the water from the eastern Beaufort Sea. However, it should be stressed that in a time-dependent, turbulent flow field, it is impossible to unambiguously define what is inside or outside the gyre. The gyre edge defined by the lowest closed dynamic height contour has the advantage of being objective, but it is somewhat arbitrary and parcels will frequently be moving into and out of the gyre. Furthermore, the waters from the gyre and from the Barrow Canyon outflow cannot be distinguished based on the water mass properties; thus, it is difficult to quantify the contribution of the BG to the Pacific water transport in the slope current, via the westward jet on the Beaufort slope.

Our tracer study implies two different fates of the slope current. The part of the current that resides on the upper continental slope continues westward toward the East Siberian Sea, in line with the observations in Corlett and Pickart (2017) and Stabeno et al. (2018). By contrast, the portion of the current overlying deeper isobaths flows northward into the Chukchi Borderland after passing the Northwind Ridge. This is consistent with the trajectories of SOLO floats (Boury et al., 2020). Ultimately this branch gets entrained into the BG.

There remains considerable uncertainty regarding the transport across the Chukchi shelf into the interior. Our simulations suggest that the cross-shelf transport (along the 100 m isobath) integrated from 180°W to the west side of Barrow Canyon is ~0.46 Sv (not shown), much larger than the model result (0.2 Sv) in Spall et al. (2018), and inconsistent with the observationally based Chukchi shelf water mass budget of Corlett and Pickart (2017). Part of the uncertainty might be due to the stratification. The cross-shelf flow in our model exists at depths from the surface to the bottom and has a near-surface velocity maximum, corresponding to the highly stratified structure of density. This is different than in the model of Spall et al. (2018) where the ocean is less stratified and the off-shelf flux is concentrated near the bottom Ekman layer (related to the eastward shelfbreak jet). We note that the Chukchi shelfbreak jet in our model is not well represented (see Figure 5b). In addition, the off-shelf transport in the model appears to be sensitive to the ice-ocean stress. For example, when masking out the ice-ocean stress over the Chukchi slope region, more of the water flows northward through Barrow Canyon rather than crossing the shelf west of the canyon. In response

to this, the slope current becomes surface-intensified (even in winter and spring) and transports more outflowing water from the canyon toward the west. Further studies are required to improve our understanding of the effects of ice-ocean stress on the off-shelf transport as well as the structure of the slope current.

Data Availability Statement

Data of volume, heat, and freshwater fluxes through Bering Strait are available at http://psc.apl.washington.edu/HLD/Bstrait/Data/BeringStraitMooringDataArchive.html. The Barrow Canyon mooring data can be found at http://www.jamstec.go.jp/arctic/data_archive_work/mooring/mooring_dl.html. The Chukchi slope mooring data are available through the Bureau of Ocean and Energy Management (https://www.boem.gov). The Chukchi slope hydrographic and shipboard ADCP data are available through http://hdl.handle.net/1912/8170. Polar science center Hydrographic Climatology (PHC) 3.0 Product II (winter fields) can be found at http://psc.apl.washington.edu/nonwp_projects/PHC/Data3.html. Polar Science Center Global Sea Ice (GIOMAS) Data Sets are available at http://psc.apl.uw.edu/data/global-sea-ice-giomas-data-sets/. The product of Estimating the Circulation and Climate of the Ocean, Phase II (ECCO2) is available at https://ecco-group.org/products.htm. Japanese 55-year Reanalysis (JRA-55) data set can be found at https://rda.ucar.edu/datasets/ds628.1. The monthly mean river runoff from the Regional, Electronic, Hydrographic Data Network for the Arctic Region (R-ArcticNET) is available at https://www.r-arcticnet.sr.unh.edu/v4.0/AllData/index.html. The numerical model input parameters, forcing fields, configuration and model results are stored at http://doi.org/10.5281/zenodo.4287714.

Acknowledgments
This work was funded by the National Key Research and Development Program of China (Grant 2017YFA0604600), the Fundamental Research Funds for the Central Universities (Grant 2019B81214), the National Natural Science Foundation of China (Grant 41676019), the Postgraduate Research & Practice Innovation Program of Jiangsu Province (Grant KYCX19_0384), the National Science Foundation (Grants OPP-1822334, PLR-1504333 and OPP-1733564), and the National Oceanic and Atmospheric Administration (Grant NA14OAR4320158). H. Leng was also supported by the scholarship from China Scholarship Council (Grant 201906710152). The authors thank the two reviewers for their helpful comments and suggestions.

References

Aagaard, K., & Carmack, E. C. (1989). The role of sea ice and other fresh water in the Arctic circulation. *Journal of Geophysical Research*, *94*(C10), 14485–14498. https://doi.org/10.1029/jc094ic10p14485

Adcroft, A., & Campin, J.-M. (2004). Rescaled height coordinates for accurate representation of free-surface flows in ocean circulation models. *Ocean Modelling*, *7*(3), 269–284. https://doi.org/10.1016/j.ocemod.2003.09.003

Adcroft, A., Hill, C., & Marshall, J. (1997). Representation of topography by shaved cells in a height coordinate ocean model. *Monthly Weather Review*, *125*, 2293–2315. https://doi.org/10.1175/1520-0493(1997)125<2293:rotbsc>2.0.co;2

Bareiss, J., Eicken, H., Helbig, A., & Martin, T. (1999). Impact of river discharge and regional climatology on the decay of sea ice in the Laptev Sea during spring and early summer. *Arctic Antarctic and Alpine Research*, *31*, 214–229. https://doi.org/10.1080/15230430.1999.12003302

Bourgain, P., & Gascard, J. C. (2012). The Atlantic and summer Pacific waters variability in the Arctic Ocean from 1997 to 2008. *Geophysical Research Letters*, *39*, L05603. https://doi.org/10.1029/2012gl051045

Boury, S., Pickart, R. S., Odier, P., Lin, P., Li, M., Fine, E. C., et al. (2020). Whither the Chukchi Slope Current? *Journal of Physical Oceanography*, *50*, 1717–1732. https://doi.org/10.1175/jpo-d-19-0273.1

Campin, J.-M., Marshall, J., & Ferreira, D. (2008). Sea ice-ocean coupling using a rescaled vertical coordinate z. *Ocean Modelling*, *24*(12), 1–14. https://doi.org/10.1016/j.ocemod.2008.05.005

Coachman, L. K., Aagaard, K., & Tripp, R. B. (1975). *Bering Strait: The regional physical oceanography*. Seattle: University of Washington Press

Coachman, L. K., & Barnes, C. A. (1961). The contribution of Bering Sea Water to the Arctic Ocean. *Arctic*, *14*, 147–161. https://doi.org/10.14430/arctic3670

Corlett, W. B., & Pickart, R. S. (2017). The Chukchi slope current. *Progress in Oceanography*, *153*, 50–65. https://doi.org/10.1016/j.pocean.2017.04.005

Cross, J. N., Mathis, J. T., Pickart, R. S., & Bates, N. R. (2018). Formation and transport of corrosive water in the Pacific Arctic region. *Deep Sea Research Part II: Topical Studies in Oceanography*, *152*, 67–81. https://doi.org/10.1016/j.dsr2.2018.05.020

Daru, V., & Tenaud, C. (2004). High order one-step monotonicity-preserving schemes for unsteady compressible flow calculations. *Journal of Computational Physics*, *193*(2), 563–594. https://doi.org/10.1016/j.jcp.2003.08.023

Fang, Y. -C., Weingartner, T. J., Dobbins, E. L., Winsor, P., Statscewich, H., Potter, R. A., et al. (2020). Circulation and thermohaline variability of the Hanna Shoal region on the northeastern Chukchi Sea shelf. *Journal of Geophysical Research: Oceans*, *125*, e2019JC015639. https://doi.org/10.1029/2019jc015639

Fox-Kemper, B., & Menemenlis, D. (2008). Can large eddy simulation techniques improve mesoscale rich ocean models? In *Ocean modeling in an eddying regime*. (pp. 319–338). Washington, DC: AGU Geophysical Monograph.

Itoh, M., Nishino, S., Kawaguchi, Y., & Kikuchi, T. (2013). Barrow Canyon volume, heat, and freshwater fluxes revealed by long-term mooring observations between 2000 and 2008. *Journal of Geophysical Research: Oceans*, *118*(9), 4363–4379. https://doi.org/10.1002/jgrc.20290

Jackett, D. R., & McDougall, T. J. (1995). Minimal adjustment of hydrographic profiles to achieve static stability. *Journal of Atmospheric and Oceanic Technology*, *12*, 381–389. https://doi.org/10.1175/1520-0426(1995)012<0381:maohpt>2.0.co;2

Jakobsson, M., Macnab, R., Mayer, L., Anderson, R., Edwards, M., Hatzky, J., et al. (2008). An improved bathymetric portrayal of the Arctic Ocean: Implications for ocean modeling and geological, geophysical and oceanographic analyses. *Geophysical Research Letters*, *35*, L07602. https://doi.org/10.1029/2008gl033520

Kobayashi, S., Ota, Y., Harada, Y., Ebita, A., Moriya, M., Onoda, H., et al. (2015). The JRA-55 reanalysis: General specifications and basic characteristics. *Journal of the Meteorological Society of Japan*, *93*(1), 5–48. https://doi.org/10.2151/jmsj.2015-001

Lammers, R. B., Shiklomanov, A. I., Vörösmarty, C. J., Fekete, B. M., & Peterson, B. J. (2001). Assessment of contemporary Arctic river runoff based on observational discharge records. *Journal of Geophysical Research*, *106*(D4), 3321–3334. https://doi.org/10.1029/2000jd900444

Large, W. G., McWilliams, J. C., & Doney, S. C. (1994). Oceanic vertical mixing: A review and a model with a nonlocal boundary layer parameterization. *Reviews of Geophysics*, *32*, 363–403. https://doi.org/10.1029/94rg01872

Leith, C. E. (1996). Stochastic models of chaotic systems. *Physica D: Nonlinear Phenomena*, *98*, 481–491. https://doi.org/10.1016/0167-2789(96)00107-8

Li, M., Pickart, R. S., Spall, M. A., Weingartner, T. J., Lin, P., Moore, G. W. K., & Qi, Y. (2019). Circulation of the Chukchi Sea shelfbreak and slope from moored timeseries. *Progress in Oceanography*, *172*, 14–33. https://doi.org/10.1016/j.pocean.2019.01.002

Lin, P., Pickart, R. S., McRaven, L. T., Arrigo, K. R., Bahr, F., Lowry, K. E., et al. (2019). Water mass evolution and circulation of the northeastern Chukchi Sea in summer: Implications for nutrient distributions. *Journal of Geophysical Research: Oceans*, *124*, 4416–4432. https://doi.org/10.1029/2019jc015185

Losch, M., Menemenlis, D., Campin, J.-M., Heimbach, P., & Hill, C. (2010). On the formulation of sea-ice models. Part 1: Effects of different solver implementations and parameterizations. *Ocean Modelling*, *33*, 129–144. https://doi.org/10.1016/j.ocemod.2009.12.008

Marks, K. M., & Smith, W. H. F. (2006). An evaluation of publicly available global bathymetry grids. *Marine Geophysical Researches*, *27*, 19–34. https://doi.org/10.1007/s11001-005-2095-4

Marshall, J., Hill, C., Perelman, L., & Adcroft, A. (1997). Hydrostatic, quasi-hydrostatic, and nonhydrostatic ocean modeling. *Journal of Geophysical Research*, *102*(C3), 5733–5752. https://doi.org/10.1029/96jc02776

McLaughlin, F. A., Carmack, E. C., Macdonald, R. W., & Bishop, J. K. B. (1996). Physical and geochemical properties across the Atlantic/Pacific water mass front in the southern Canadian Basin. *Journal of Geophysical Research*, *101*, 1183–1197. https://doi.org/10.1029/95jc02634

Menemenlis, D., Campin, J.-M., Heimbach, P., Hill, C., Lee, T., Nguyen, A., et al. (2008). ECCO2: High resolution global ocean and sea ice data synthesis. *Mercator Ocean Quarterly Newsletter*, *31*, 13–21.

Nguyen, A. T., Kwok, R., & Menemenlis, D. (2012). Source and pathway of the western Arctic upper halocline in a data-constrained coupled ocean and sea ice model. *Journal of Physical Oceanography*, *42*(5), 802–823. https://doi.org/10.1175/jpo-d-11-040.1

Nguyen, A. T., Menemenlis, D., & Kwok, R. (2009). Improved modeling of the Arctic halocline with a subgrid-scale brine rejection parameterization. *Journal of Geophysical Research*, *114*, C11014. https://doi.org/10.1029/2008jc005121

Nikolopoulos, A., Pickart, R. S., Fratantoni, P. S., Shimada, K., Torres, D. J., & Jones, E. P. (2009). The western Arctic boundary current at 152°W: Structure, variability, and transport. *Deep Sea Research Part II: Topical Studies in Oceanography*, *56*, 1164–1181. https://doi.org/10.1016/j.dsr2.2008.10.014

Nummelin, A., Li, C., & Smedsrud, L. H. (2015). Response of Arctic Ocean stratification to changing river runoff in a column model. *Journal of Geophysical Research: Oceans*, *120*, 2655–2675. https://doi.org/10.1002/2014jc010571

Panteleev, G., Nechaev, D. A., Proshutinsky, A., Woodgate, R. A., & Zhang, J. (2010). Reconstruction and analysis of the Chukchi Sea circulation in 1990–1991. *Journal of Geophysical Research*, *115*(8), 1–22. https://doi.org/10.1029/2009jc005453

Paquette, R. G., & Bourke, R. H. (1974). Observations on the coastal current of Arctic Alaska. *Journal of Marine Research*, *32*, 195–207.

Pickart, R. S. (2004). Shelfbreak circulation in the Alaskan Beaufort Sea: Mean structure and variability. *Journal of Geophysical Research*, *109*, C04024. https://doi.org/10.1029/2003jc001912

Pickart, R. S., Moore, G. W. K., Mao, C., Bahr, F., Nobre, C., & Weingartner, T. J. (2016). Circulation of winter water on the Chukchi shelf in early summer. *Deep Sea Research Part II: Topical Studies in Oceanography*, *57*. https://doi.org/10.1016/j.dsr2.2016.05.001

Pickart, R. S., Pratt, L. J., Torres, D. J., Whitledge, T. E., Proshutinsky, A. Y., Aagaard, K., et al. (2010). Evolution and dynamics of the flow through herald canyon in the western Chukchi Sea. *Deep Sea Research Part II: Topical Studies in Oceanography*, *57*, 5–26. https://doi.org/10.1016/j.dsr2.2009.08.002

Proshutinsky, A., Bourke, R. H., & McLaughlin, F. A. (2002). The role of the Beaufort Gyre in Arctic climate variability: Seasonal to decadal climate scales. *Geophysical Research Letters*, *29*(23), 2100. https://doi.org/10.1029/2002gl015847

Proshutinsky, A., Krishfield, R., Timmermans, M.-L., Toole, J., Carmack, E., McLaughlin, F., et al. (2009). Beaufort Gyre freshwater reservoir: State and variability from observations. *Journal of Geophysical Research*, *114*, C00A10. https://doi.org/10.1029/2008jc005104

Qi, D., Chen, L., Chen, B., Gao, Z., Zhong, W., Feely, R. A., et al. (2017). Increase in acidifying water in the western Arctic Ocean. *Nature Climate Change*, *7*(3), 195–199. https://doi.org/10.1038/nclimate3228

Regan, H. C., Lique, C., & Armitage, T. W. K. (2019). The Beaufort Gyre extent, shape, and location between 2003 and 2014 from satellite observations. *Journal of Geophysical Research: Oceans*, *124*, 844–862. https://doi.org/10.1029/2018jc014379

Serreze, M. C., Barrett, A. P., Slater, A. G., Woodgate, R. A., Aagaard, K., Lammers, R. B., et al. (2006). The large-scale freshwater cycle of the Arctic. *Journal of Geophysical Research*, *111*, C11010. https://doi.org/10.1029/2005jc003424

Serreze, M. C., Crawford, A. D., Stroeve, J. C., Barrett, A. P., & Woodgate, R. A. (2016). Variability, trends, and predictability of seasonal sea ice retreat and advance in the Chukchi Sea. *Journal of Geophysical Research: Oceans*, *121*, 7308–7325. https://doi.org/10.1002/2016jc011977

Shiklomanov, A. I., Yakovleva, T. I., Lammers, R. B., Karasev, I. P., Vörösmarty, C. J., & Linder, E. (2006). Cold region river discharge uncertainty-estimates from large Russian rivers. *Journal of Hydrology*, *326*(1–4), 231–256. https://doi.org/10.1016/j.jhydrol.2005.10.037

Shimada, K., Kamoshida, T., Itoh, M., Nishino, S., Carmack, E., McLaughlin, F. A., et al. (2006). Pacific Ocean inflow: Influence on catastrophic reduction of sea ice cover in the Arctic Ocean. *Geophysical Research Letters*, *33*, L08605. https://doi.org/10.1029/2005gl025624

Spall, M. A. (2007). Circulation and water mass transformation in a model of the Chukchi Sea. *Journal of Geophysical Research*, *112*, C05025. https://doi.org/10.1029/2005jc003364

Spall, M. A., Pickart, R. S., Li, M., Itoh, M., Lin, P., Kikuchi, T., & Qi, Y. (2018). Transport of Pacific water into the Canada basin and the formation of the Chukchi slope current. *Journal of Geophysical Research: Oceans*, *123*, 7453–7471. https://doi.org/10.1029/2018jc013825

Stabeno, P., Kachel, N., Ladd, C., & Woodgate, R. (2018). Flow Patterns in the Eastern Chukchi Sea: 2010–2015. *Journal of Geophysical Research: Oceans*, *123*, 1177–1195. https://doi.org/10.1002/2017jc013135

Stabeno, P. J., & McCabe, R. M. (2020). Vertical structure and temporal variability of currents over the Chukchi Sea continental slope. *Deep Sea Research Part II: Topical Studies in Oceanography*, *177*, 0967–0645. https://doi.org/10.1016/j.dsr2.2020.104805

Steele, M., Morison, J., Ermold, W., Rigor, I., Ortmeyer, M., & Shimada, K. (2004). Circulation of summer Pacific halocline water in the Arctic Ocean. *Journal of Geophysical Research*, *109*, C02027. https://doi.org/10.1029/2003jc002009

Steele, M., Morley, R., & Ermold, W. (2001). PHC: A global ocean hydrography with a high-quality Arctic Ocean. *Journal of Climate*, *14*, 2079–2087. https://doi.org/10.1175/1520-0442(2001)014<2079:pagohw>2.0.co;2

Timmermans, M. L., Proshutinsky, A., Golubeva, E., Jackson, J. M., Krishfield, R., McCall, M., et al. (2014). Mechanisms of Pacific Summer Water variability in the Arctic's Central Canada Basin. *Journal of Geophysical Research: Oceans*, *119*, 7523–7548. https://doi.org/10.1002/2014jc010273

Watanabe, E., Onodera, J., Itoh, M., Nishino, S., & Kikuchi, T. (2017). Winter transport of subsurface warm water toward the Arctic Chukchi Borderland. *Deep Sea Research Part I: Oceanographic Research Papers*, *128*, 115–130. https://doi.org/10.1016/j.dsr.2017.08.009

Weingartner, T., Aagaard, K., Woodgate, R., Danielson, S., Sasaki, Y., & Cavalieri, D. (2005). Circulation on the north central Chukchi Sea shelf. *Deep Sea Research Part II: Topical Studies in Oceanography*, *52*, 3150–3174. https://doi.org/10.1016/j.dsr2.2005.10.015

Winsor, P., & Chapman, D. C. (2004). Pathways of Pacific water across the Chukchi Sea: A numerical model study. *Journal of Geophysical Research*, *109*, C03002. https://doi.org/10.1029/2003jc001962

Woodgate, R., Stafford, K., & Prahl, F. (2015). A Synthesis of year-round interdisciplinary mooring measurements in the Bering Strait (1990–2014) and the RUSALCA years (2004–2011). *Oceanography*, *28*(3), 46–67. https://doi.org/10.5670/oceanog.2015.57

Woodgate, R. A. (2018). Increases in the Pacific inflow to the Arctic from 1990 to 2015, and insights into seasonal trends and driving mechanisms from year-round Bering Strait mooring data. *Progress in Oceanography*, *160*, 124–154. https://doi.org/10.1016/j.pocean.2017.12.007

Woodgate, R. A., Aagaard, K., & Weingartner, T. J. (2005). A year in the physical oceanography of the Chukchi Sea: Moored measurements from autumn 1990-1991. *Deep Sea Research Part II: Topical Studies in Oceanography*, *52*(24–26), 3116–3149. https://doi.org/10.1016/j.dsr2.2005.10.016

Woodgate, R. A., Weingartner, T. J., & Lindsay, R. (2012). Observed increases in Bering Strait oceanic fluxes from the Pacific to the Arctic from 2001 to 2011 and their impacts on the Arctic Ocean water column. *Geophysical Research Letters*, *39*(24), 6. https://doi.org/10.1029/2012gl054092

Zhang, J., & Hibler, W. D. (1997). On an efficient numerical method for modeling sea ice dynamics. *Journal of Geophysical Research*, *102*(C4), 8691–8702. https://doi.org/10.1029/96jc03744

Zhang, J., & Rothrock, D. (2003). Modeling global sea ice with a thickness and enthalpy distribution model in generalized curvilinear coordinates. *Monthly Weather Review*, *131*, 681–697. https://doi.org/10.1175/1520-0493(2003)131<0845:mgsiwa>2.0.co;2

Zhao, M., Timmermans, M.-L., Cole, S., Krishfield, R., Proshutinsky, A., & Toole, J. (2014). Characterizing the eddy field in the arctic ocean halocline. *Journal of Geophysical Research: Oceans*, *119*, 8800–8817. https://doi.org/10.1002/2014jc010488